A Novel Wavenumber Domain Algorithm for Bistatic SAR Imaging Based on Equivalent Monostatic Model

Zongliang Wu*, Xiaoling Zhang, and Xiliang Wu

Abstract—Compared with traditional monostatic synthetic aperture radar (SAR), bistatic SAR (BiSAR) has stronger advantages in terms of anti-interference and anti-strike abilities. However, the complex system structure of BiSAR brings new difficulties to imaging processing. In order to make the imaging algorithms of traditional monostatic SAR apply to BiSAR imaging as well, this paper proposes an equivalent monostatic model for BiSAR. This model mainly provides two benefits: (1) The equivalent monostatic range history has the form of hyperbolic function; (2) The equivalent monostatic velocity of any scattering point in the observed scene, with respect to the radar platform, is not only the same but also invariant with the equivalent monostatic range. Due to the above benefits, a novel wavenumber domain algorithm (WDA) is further proposed for BiSAR imaging. Finally, the experimental results demonstrate that the proposed algorithm is effective and feasible.

1. INTRODUCTION

At present, bistatic synthetic aperture radar (BiSAR) is widely used in practice. Relative to traditional monostatic SAR, BiSAR can obtain more abundant scattering information for imaging targets, and it also has stronger anti-interference and anti-strike abilities. However, the complex system structure of BiSAR brings new challenges to imaging processing. Compared with other conventional SAR imaging algorithms, such as range-Doppler algorithm (RDA) [1–3] and chirp scaling algorithm (CSA) [4–6], wavenumber domain algorithm (WDA) [7–9] can perform accurate imaging for all squint angles and all aperture lengths, so long as the range history can be denoted as the hyperbolic function, and the radial velocity, with respect to the radar platform, is invariant with the range. When applying WDA to BiSAR imaging, the prior condition is to acquire the accurate two-dimensional (2D) spectrum.

Owing to the fact that the range history of BiSAR is no longer the form of hyperbolic function, it is not available to employ the principle of stationary phase (POSP) to directly deduce the analytical 2D spectrum of BiSAR. Based on the principle of least squares [10, 11], this paper proposes an equivalent monostatic range history model for BiSAR. This model is referred to as the equivalent monostatic SAR. It mainly has two advantages: on the one hand, the range history of the equivalent monostatic SAR can be expressed in the form of hyperbolic function; on the other hand, the radial velocity of the equivalent monostatic SAR is fixed and invariant with the equivalent monostatic range. For the above advantages, the 2D spectrum of BiSAR can be computed conveniently. Ultimately, according to the computed 2D spectrum, a novel WDA is proposed for BiSAR imaging.

2. EQUIVALENT MONOSTATIC MODEL FOR BISAR

The geometric structure of BiSAR is depicted in Fig. 1, where **X**-**Y**-**Z** denotes the reference coordinate system, and **O** is the coordinate origin; the subscripts T and R represent the transmitter and receiver,
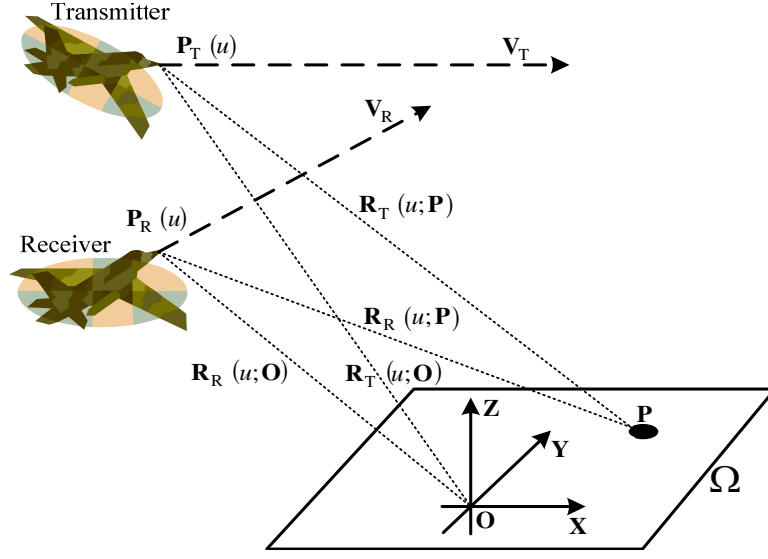
Figure 1. The geometric structure of BiSAR.

respectively; u denotes the slow-time; assume that $\mathbf{\Omega}$ denotes the observed scene, and $\mathbf{P}(\mathbf{P} \in \mathbf{\Omega})$ is a scattering point. When $u = 0$, the spatial locations of the transmitter and receiver are expressed as

$$\begin{cases} \mathbf{P}_{0\mathrm{T}} = [x_{0\mathrm{T}} \quad y_{0\mathrm{T}} \quad z_{\mathrm{T}}]^{\mathrm{T}} \\ \mathbf{P}_{0\mathrm{R}} = [x_{0\mathrm{R}} \quad y_{0\mathrm{R}} \quad z_{\mathrm{R}}]^{\mathrm{T}} \end{cases} \tag{1}$$

The velocity vectors of the transmitter and receiver are defined as

$$\begin{cases} \mathbf{V}_{\mathrm{T}} = [v_{x\mathrm{T}} \quad v_{y\mathrm{T}} \quad 0]^{\mathrm{T}} \\ \mathbf{V}_{\mathrm{R}} = [v_{x\mathrm{R}} \quad v_{y\mathrm{R}} \quad 0]^{\mathrm{T}} \end{cases} \tag{2}$$

According to Eq. (1) and Eq. (2), it is easy to calculate the locations of the transmitter and receiver at slow-time u, namely

$$\begin{cases} \mathbf{P}_{\mathrm{T}}(u) = \mathbf{P}_{0\mathrm{T}} + \mathbf{V}_{\mathrm{T}} \cdot u \\ \mathbf{P}_{\mathrm{R}}(u) = \mathbf{P}_{0\mathrm{R}} + \mathbf{V}_{\mathrm{R}} \cdot u \end{cases} \tag{3}$$

where $-T/2 \leq u \leq T/2$ (T denotes the synthetic aperture time).

Assume that the scattering point $\mathbf{P}$ is located at $\mathbf{P} = [x \ y \ z]^{\mathrm{T}}$, so the range histories of the transmitter and receiver with respect to $\mathbf{P}$ are obtained by

$$\begin{cases} R_{\mathrm{T}}(u; \mathbf{P}) = \|\mathbf{P}_{\mathrm{T}}(u) - \mathbf{P}\| = \sqrt{\|\mathbf{V}_{\mathrm{T}}\|^2 \cdot u^2 + 2\mathbf{V}_{\mathrm{T}}^{\mathrm{T}}(\mathbf{P}_{0\mathrm{T}} - \mathbf{P}) \cdot u + \|\mathbf{P}_{0\mathrm{T}} - \mathbf{P}\|^2} \\ R_{\mathrm{R}}(u; \mathbf{P}) = \|\mathbf{P}_{\mathrm{R}}(u) - \mathbf{P}\| = \sqrt{\|\mathbf{V}_{\mathrm{R}}\|^2 \cdot u^2 + 2\mathbf{V}_{\mathrm{R}}^{\mathrm{T}}(\mathbf{P}_{0\mathrm{R}} - \mathbf{P}) \cdot u + \|\mathbf{P}_{0\mathrm{R}} - \mathbf{P}\|^2} \end{cases} \tag{4}$$

where $\|\cdot\|$ denotes the 2-norm of vector. Via Eq. (4), the range history $R(u; \mathbf{P})$ of BiSAR is as follows:

$$\begin{aligned} R(u; \mathbf{P}) &= R_{\mathrm{T}}(u; \mathbf{P}) + R_{\mathrm{R}}(u; \mathbf{P}) \\ &= \sqrt{\|\mathbf{V}_{\mathrm{T}}\|^2 \cdot u^2 + 2\mathbf{V}_{\mathrm{T}}^{\mathrm{T}}(\mathbf{P}_{0\mathrm{T}} - \mathbf{P}) \cdot u + \|\mathbf{P}_{0\mathrm{T}} - \mathbf{P}\|^2} \\ &\quad + \sqrt{\|\mathbf{V}_{\mathrm{R}}\|^2 \cdot u^2 + 2\mathbf{V}_{\mathrm{R}}^{\mathrm{T}}(\mathbf{P}_{0\mathrm{R}} - \mathbf{P}) \cdot u + \|\mathbf{P}_{0\mathrm{R}} - \mathbf{P}\|^2} \end{aligned} \tag{5}$$

From Eq. (5), the range history of BiSAR has the form of double square root (DSR), and it is much different from that of traditional monostatic SAR (The range history of traditional monostatic SAR has the form of hyperbolic function).

For monostatic SAR, its transmitter and receiver are both identical, thus they have the same position and velocity vector:

$$\mathbf{P}_{0T} = \mathbf{P}_{0R} = \mathbf{P}_0 \tag{6}$$

$$\mathbf{V}_T = \mathbf{V}_R = \mathbf{V} \tag{7}$$

Substituting Eq. (6) and Eq. (7) into Eq. (5), we can acquire the range history $R_{\text{Mono}}(u; \mathbf{P})$ of monostatic SAR.

$$R_{\text{Mono}}(u; \mathbf{P}) = 2\sqrt{\|\mathbf{V}\|^2 \cdot u^2 + 2\mathbf{V}^T(\mathbf{P}_0 - \mathbf{P}) \cdot u + \|\mathbf{P}_0 - \mathbf{P}\|^2} \tag{8}$$

It is obvious that Eq. (8) has the form of hyperbolic function. Let $f(u; b_0, b_1, b_2)$ denote the general hyperbolic function, then we have

$$f(u; b_0, b_1, b_2) = \sqrt{b_0 + b_1 \cdot u + b_2 \cdot u^2} \tag{9}$$

where b_0, b_1 and b_2 are the undetermined parameters of $f(u; b_0, b_1, b_2)$.

Next, $f(u; b_0, b_1, b_2)$ and $R(u; \mathbf{P})$ are uniformly sampled on the interval $-T/2 \leq u \leq T/2$. The sampling period is the pulse repetition time. $\{u_j\}_{j=1}^N$ denote the total sampling points of u that is continuous, where N is the number of these sampling points. Through the above sampling method, $f(u; b_0, b_1, b_2)$ and $R(u; \mathbf{P})$ can be rewritten in discrete form:

$$f(u_j; b_0, b_1, b_2) = \sqrt{b_0 + b_1 \cdot u_j + b_2 \cdot u_j^2} \quad (1 \leq j \leq N) \tag{10}$$

$$R(u_j; \mathbf{P}) = R_T(u_j; \mathbf{P}) + R_R(u_j; \mathbf{P}) \quad (1 \leq j \leq N) \tag{11}$$

Via Eq. (11), the vector $\mathbf{R}(\mathbf{P}) = [R(u_1; \mathbf{P}) \quad R(u_2; \mathbf{P}) \quad \cdots \quad R(u_N; \mathbf{P})]^T$ can be obtained, which is called the range history vector of BiSAR.

Based on Eqs. (10) and (11), we build the following equation system:

$$\mathbf{U} \cdot \mathbf{b} = \mathbf{c} \tag{12}$$

where $\mathbf{b} = [b_0 \quad b_1 \quad b_2]^T$, $\mathbf{c} = [R^2(u_1; \mathbf{P}) \quad R^2(u_2; \mathbf{P}) \quad \cdots \quad R^2(u_N; \mathbf{P})]^T$, $\mathbf{U} = \begin{bmatrix} 1 & u_1 & u_1^2 \\ 1 & u_2 & u_2^2 \\ \vdots & \vdots & \vdots \\ 1 & u_N & u_N^2 \end{bmatrix}$ ($\mathbf{U}$ is

a Vandermonde matrix). By solving Eq. (12), the least squares solution of $\mathbf{b} = [b_0 \quad b_1 \quad b_2]^T$ can be acquired by

$$\mathbf{b} = [\mathbf{U}^H \mathbf{U}]^{-1} \mathbf{U}^H \mathbf{c} \tag{13}$$

where $[\mathbf{U}^H \mathbf{U}]^{-1}$ denotes the inverse matrix of $\mathbf{U}^H \mathbf{U}$, and $[\mathbf{U}^H \mathbf{U}]^{-1} \mathbf{U}^H$ denotes the pseudo-inverse matrix of $\mathbf{U}$.

The concrete formulas in regard to b_0, b_1 and b_2 are given below.

$$\begin{cases} b_0 = \sum_{j=1}^N \alpha_{0,j} R^2(u_j; \mathbf{P}) \\ b_1 = \sum_{j=1}^N \alpha_{1,j} R^2(u_j; \mathbf{P}) \\ b_2 = \sum_{j=1}^N \alpha_{2,j} R^2(u_j; \mathbf{P}) \end{cases} \tag{14}$$

$$\begin{cases} \alpha_{0,j} = \sum_{q=0}^{2} \beta_{0,q} u_j^q \\[2mm] \alpha_{1,j} = \sum_{q=0}^{2} \beta_{1,q} u_j^q \\[2mm] \alpha_{2,j} = \sum_{q=0}^{2} \beta_{2,q} u_j^q \end{cases} \tag{15}$$

In Eq. (15), $q = 0, 1, 2$; $\beta_{0,q}$ is the element of $\left[\mathbf{U}^{\mathrm{H}}\mathbf{U}\right]^{-1}$ at the first row and the $(q + 1)$th column; $\beta_{1,q}$ is the element of $\left[\mathbf{U}^{\mathrm{H}}\mathbf{U}\right]^{-1}$ at the second row and the $(q + 1)$th column; $\beta_{2,q}$ is the element of $\left[\mathbf{U}^{\mathrm{H}}\mathbf{U}\right]^{-1}$ at the third row and the $(q + 1)$th column. Since $\mathbf{U}$ is a Vandermonde matrix, $\left[\mathbf{U}^{\mathrm{H}}\mathbf{U}\right]^{-1}$ must exist. The parameters b_0, b_1 and b_2 obtained by Eq. (14) and Eq. (15) are optimal in the sense of least squares.

Then combining Eq. (8) with Eq. (9), the equivalent monostatic range history $\hat{R}_{\mathrm{Mono}}(u; \mathbf{P})$ for BiSAR is represented as

$$\hat{R}_{\mathrm{Mono}}(u; \mathbf{P}) = 2\sqrt{r_0^2(\mathbf{P}) - 2Vr_0(\mathbf{P})\sin\theta(\mathbf{P}) \cdot u + V^2 \cdot u^2} \tag{16}$$

The mathematic model defined by Eq. (16) is referred to as the equivalent monostatic SAR, and $\hat{R}_{\mathrm{Mono}}(u; \mathbf{P})$ is called the range history of the equivalent monostatic SAR. In Eq. (16), V is the equivalent monostatic velocity; $r_0(\mathbf{P})$ is the initial range of the equivalent monostatic SAR; $\theta(\mathbf{P})$ is the initial squint angle of the equivalent monostatic SAR. V, $r_0(\mathbf{P})$ and $\theta(\mathbf{P})$ have the following expressions:

$$V = \frac{1}{2}\sqrt{\sum_{j=1}^{N} \alpha_{2,j} R^2(u_j; \mathbf{O})} \tag{17}$$

$$r_0(\mathbf{P}) = \frac{1}{2}\sqrt{\sum_{j=1}^{N} \alpha_{0,j} R^2(u_j; \mathbf{P})} \tag{18}$$

$$\theta(\mathbf{P}) = \arcsin\left(-\frac{\sum_{j=1}^{N} \alpha_{1,j} R^2(u_j; \mathbf{P})}{8Vr_0(\mathbf{P})}\right) \tag{19}$$

From Eqs. (16) and (17), the range history $\hat{R}_{\mathrm{Mono}}(u; \mathbf{P})$ of the equivalent monostatic SAR has the form of hyperbolic function, and the equivalent monostatic velocity V is a constant invariant with $\hat{R}_{\mathrm{Mono}}(u; \mathbf{P})$. These results will be helpful for deriving the 2D spectrum of BiSAR.

The approximation error $e(u; \mathbf{P})$ of $\hat{R}_{\mathrm{Mono}}(u; \mathbf{P})$ is defined by

$$e(u; \mathbf{P}) = \hat{R}_{\mathrm{Mono}}(u; \mathbf{P}) - R(u; \mathbf{P}) \tag{20}$$

According to $e(u; \mathbf{P})$, we can obtain the following constraints [12]:

$$\max_{\substack{-T/2 \leq u \leq T/2 \\ \mathbf{P} \in \mathbf{\Omega}}} |e(u; \mathbf{P})| \leq \frac{\lambda}{4} \tag{21}$$

where $|e(u; \mathbf{P})|$ denotes the absolute value of $e(u; \mathbf{P})$, and λ denotes the wavelength of the carrier wave. If the scattering point $\mathbf{P}$ satisfies Eq. (21), $e(u; \mathbf{P})$ has little influence on the final imaging result, which can be neglected. In other words, when Eq. (21) is satisfied, the equivalent monostatic SAR model is accurate. So long as all scattering points in the observed scene $\mathbf{\Omega}$ satisfy Eq. (21), BiSAR can be transformed into the equivalent monostatic SAR. Further, we are able to use the imaging algorithms of traditional monostatic SAR to focus the echo data of BiSAR.

3. NOVEL WAVENUMBER DOMAIN ALGORITHM FOR BISAR IMAGING

Based on the information in the previous section, the range history $\hat{R}_{\text{Mono}}(u; \mathbf{P})$ (see Eq. (16)) has the form of hyperbolic function, and the equivalent monostatic velocity V (see Eq. (17)) is independent of $\hat{R}_{\text{Mono}}(u; \mathbf{P})$. These conclusions are in favor of using wavenumber domain algorithm (WDA) to achieve imaging. In this section, a novel WDA is proposed for BiSAR imaging.

Similar to traditional monostatic SAR, we directly provide the 2D spectrum $S(f, f_u)$ of the equivalent monostatic SAR. Although this 2D spectrum is similar with that of traditional monostaitc SAR, some important parameters need to be redefined. $S(f, f_u)$ is expressed as

$$S(f, f_u) = \int_{\boldsymbol{\Omega}} \sigma(\mathbf{P}) \exp\left(-j4\pi \frac{r_b(\mathbf{P})}{c}\sqrt{(f_c + f)^2 - \frac{c^2 f_u^2}{4V^2}} - j2\pi \frac{x(\mathbf{P})}{V} f_u\right) d\mathbf{P} \tag{22}$$

where f is the frequency corresponding to the fast-time, called fast-frequency; f_u is the frequency corresponding to the slow-time, called slow-frequency; $\boldsymbol{\Omega}$ is the observed scene; $\sigma(\mathbf{P})$ denotes the backscattering coefficient of the scattering point $\mathbf{P}$; c denotes the propagation speed of the electromagnetic wave; f_c denotes the carrier frequency; V is the equivalent monostatic velocity; $r_b(\mathbf{P})$ and $x(\mathbf{P})$ are as follows:

$$r_b(\mathbf{P}) = r_0(\mathbf{P})\cos\theta(\mathbf{P}) \tag{23}$$

$$x(\mathbf{P}) = r_0(\mathbf{P})\sin\theta(\mathbf{P}) \tag{24}$$

where $r_0(\mathbf{P})$ and $\theta(\mathbf{P})$ (see Eq. (18) and Eq. (19)) are the initial range and initial squint angle of the equivalent monostatic SAR, respectively.

The reference function $S_{\text{ref}}(f, f_u)$ is defined by

$$S_{\text{ref}}(f, f_u) = \exp\left(-j4\pi \frac{r_b(\mathbf{O})}{c}\sqrt{(f_c + f)^2 - \frac{c^2 f_u^2}{4V^2}} - j2\pi \frac{x(\mathbf{O})}{V} f_u\right) \tag{25}$$

where $\mathbf{O}$ is the coordinate origin. Then multiplying $S(f, f_u)$ with the conjugate of $S_{\text{ref}}(f, f_u)$, the 2D spectrum $S_{\text{RFM}}(f, f_u)$ is acquired.

$$\begin{aligned} S_{\text{RFM}}(f, f_u) &= S(f, f_u) S_{\text{ref}}^*(f, f_u) \\ &= \int_{\boldsymbol{\Omega}} \sigma(\mathbf{P}) \exp\left(-j4\pi \frac{\Delta r_b(\mathbf{P})}{c}\sqrt{(f_c + f)^2 - \frac{c^2 f_u^2}{4V^2}} - j2\pi \frac{\Delta x(\mathbf{P})}{V} f_u\right) d\mathbf{P} \end{aligned} \tag{26}$$

where $S_{\text{ref}}^*(f, f_u)$ denotes the conjugate of $S_{\text{ref}}(f, f_u)$; $\Delta r_b(\mathbf{P})$ and $\Delta x(\mathbf{P})$ have the following expressions:

$$\Delta r_b(\mathbf{P}) = r_b(\mathbf{P}) - r_b(\mathbf{O}) \tag{27}$$

$$\Delta x(\mathbf{P}) = x(\mathbf{P}) - x(\mathbf{O}) \tag{28}$$

Next, we employ Stolt transform [12] to handle Eq. (26), that is, a new fast-frequency f' is redefined.

$$f' = \sqrt{(f_c + f)^2 - \frac{c^2 f_u^2}{4V^2}} - f_c \tag{29}$$

From Eq. (29), the 2D spectrum $S_{\text{RFM}}(f, f_u)$ is rewritten as

$$S'_{\text{RFM}}(f', f_u) = \int_{\boldsymbol{\Omega}} \sigma(\mathbf{P}) \exp\left(-j4\pi \frac{\Delta r_b(\mathbf{P})}{c}(f_c + f') - j2\pi \frac{\Delta x(\mathbf{P})}{V} f_u\right) d\mathbf{P} \tag{30}$$

Once $S'_{\text{RFM}}(f', f_u)$ is obtained, the imaging processing can be carried out. Firstly, $S'_{\text{RFM}}(f', f_u)$ is resampled with respect to the fast-frequency f'. Secondly, we take the operation of inverse fast Fourier transform (IFFT) successively on the fast-frequency f' and slow-frequency f_u. After accomplishing the two steps, a focused BiSAR image can be gotten.

In order to evaluate the focusing level of the novel WDA proposed by this paper, a concept of the matching ratio is introduced below. Similar to the generating method of the range history vector $\mathbf{R}(\mathbf{P})$ of

BiSAR in Section 2, the vectors $\hat{\mathbf{R}}_{\mathrm{Mono}}(\mathbf{P}) = \left[\hat{R}_{\mathrm{Mono}}(u_1; \mathbf{P}) \quad \hat{R}_{\mathrm{Mono}}(u_2; \mathbf{P}) \quad \cdots \quad \hat{R}_{\mathrm{Mono}}(u_N; \mathbf{P}) \right]^{\mathrm{T}}$ and $\mathbf{e}(\mathbf{P}) = \left[e(u_1; \mathbf{P}) \quad e(u_2; \mathbf{P}) \quad \cdots \quad e(u_N; \mathbf{P}) \right]^{\mathrm{T}}$ can be acquired respectively by uniformly sampling $\hat{R}_{\mathrm{Mono}}(u; \mathbf{P})$ and $e(u; \mathbf{P})$ on the interval $-T/2 \leq u \leq T/2$. $\hat{\mathbf{R}}_{\mathrm{Mono}}(\mathbf{P})$ is called the range history vector of the equivalent monostatic SAR, and $\mathbf{e}(\mathbf{P})$ is called the approximation error vector.

According to the vectors $\mathbf{e}(\mathbf{P})$, $\hat{\mathbf{R}}_{\mathrm{Mono}}(\mathbf{P})$ and $\mathbf{R}(\mathbf{P})$, Eq. (21) is rewritten in the discrete form:

$$\max_{\substack{1 \leq j \leq N \\ \mathbf{P} \in \mathbf{\Omega}}} |e(u_j; \mathbf{P})| = \max_{\substack{1 \leq j \leq N \\ \mathbf{P} \in \mathbf{\Omega}}} \left| \hat{R}_{\mathrm{Mono}}(u_j; \mathbf{P}) - R(u_j; \mathbf{P}) \right| \leq \frac{\lambda}{4} \tag{31}$$

where $e(u_j; \mathbf{P})$ and $\hat{R}_{\mathrm{Mono}}(u_j; \mathbf{P}) - R(u_j; \mathbf{P})$ are the j-th component of $\mathbf{e}_m(\mathbf{P})$ and $\hat{\mathbf{R}}_{\mathrm{Mono}}(\mathbf{P}) - \mathbf{R}(\mathbf{P})$, respectively. Owing to Eq. (31), the following constraints can be obtained.

$$\left| \hat{R}_{\mathrm{Mono}}(u_j; \mathbf{P}) - R(u_j; \mathbf{P}) \right| \leq \frac{\lambda}{4} \quad (1 \leq j \leq N) \tag{32}$$

In this section, $N_\alpha(\mathbf{P})$ denotes the number of the components of $\hat{\mathbf{R}}_{\mathrm{Mono}}(\mathbf{P}) - \mathbf{R}(\mathbf{P})$ that satisfy Eq. (32). Since N is the number of the total components of $\hat{\mathbf{R}}_{\mathrm{Mono}}(\mathbf{P}) - \mathbf{R}(\mathbf{P})$, the matching ratio $\alpha(\mathbf{P})$ between $\hat{\mathbf{R}}_{\mathrm{Mono}}(\mathbf{P})$ and $\mathbf{R}(\mathbf{P})$ is defined as $\alpha(\mathbf{P}) = N_\alpha(\mathbf{P})/N$ $(\alpha(\mathbf{P}) \in [0,1])$.

The focusing process of WDA is essentially the coherent accumulation of pulse. For the scattering point $\mathbf{P}$, when $\alpha(\mathbf{P}) = 1$, all pulses have realized correct accumulation via the novel WDA during a synthetic aperture time. Therefore, when $\alpha(\mathbf{P}) = 1$, the novel WDA has achieved accurate focusing for $\mathbf{P}$, at this time $\hat{\mathbf{R}}_{\mathrm{Mono}}(\mathbf{P})$ and $\mathbf{R}(\mathbf{P})$ reach complete matching. Via the matching ratio $\alpha(\mathbf{P})$, we can conclude: for the scattering point $\mathbf{P}$, the focusing performance of the novel WDA becomes worse and worse as $\alpha(\mathbf{P})$ decreases. The matching ratio can be regarded as a performance parameter used for evaluating the focusing level of the novel WDA. In the next section, simulation and practical experiment data of BiSAR are introduced to validate the effectiveness and correctness of the proposed imaging algorithm.

4. IMAGING EXPERIMENTS

4.1. Simulation Experiment

In this subsection, we design a simulation experiment to examine the novel WDA proposed by this paper. The simulation parameters used for BiSAR are listed in Table 1. In the observed scene, there are 5 scattering points, whose locations are shown in Fig. 2. Using the novel WDA to deal with the scene in Fig. 2, the imaging result is depicted in Fig. 3. Compared with Fig. 2, it is obvious that all the scattering points in Fig. 3 have been focused at the correct positions.

Through further calculation, the matching ratio of each scattering point in Fig. 3 is equal to 1, so the novel WDA has realized accurate focusing for all scattering points in Fig. 3. The simulation experiment verifies the novel WDA can well handle the echo data of BiSAR.

Table 1. Simulation parameters for BiSAR.

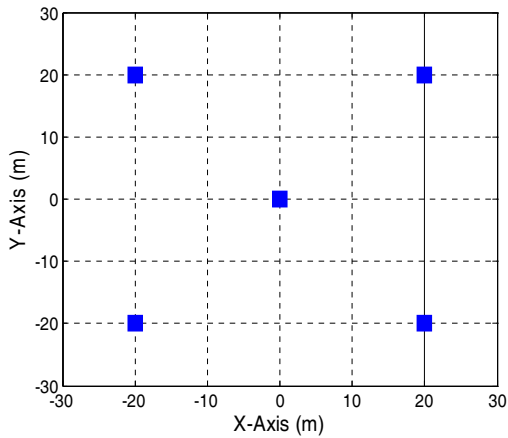| Simulation parameters	Transmitter	Receiver
Initial position (Km)	$(-0.5, -8, 8)$	$(-0.1, -3, 3)$
Platform velocity (m/s)	$(100, 0, 0)$	$(50, 100, 0)$
Carrier frequency (GHz)	10	
Sampling frequency (MHz)	200	
Range bandwidth (MHz)	150	
Pulse width (us)	2	
Pulse repetition frequency (Hz)	1000	

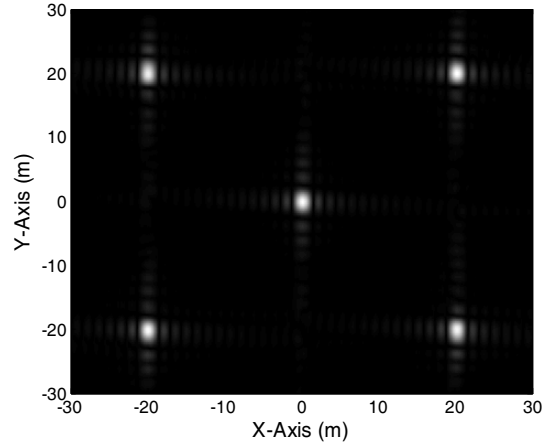**Figure 2.** The locations of the scattering points.

Figure 3. The imaging result of the simulation data from the novel WDA.

4.2. Practical Experiment

In order to further validate the imaging effect of the novel WDA, we employ the practical experiment data of airborne BiSAR. The system parameters used for airborne BiSAR are listed in Table 2. In this subsection, the practical experiment data are first focused by back projection algorithm (BPA) [13–15], and the corresponding imaging result is shown in Fig. 4. It is important to note that BPA is considered to have the best focusing performance in SAR imaging field. Then, the imaging result for the novel WDA is depicted in Fig. 5.
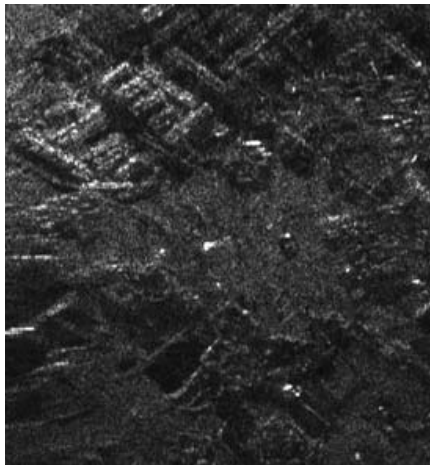

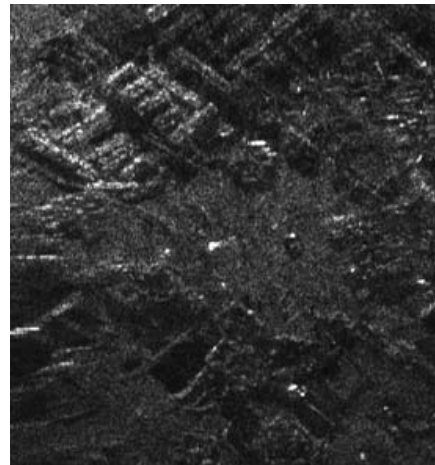**Figure 4.** The imaging result of the practical experiment data from BPA.

Figure 5. The imaging result of the practical experiment data from the novel WDA.

Through further computation, the matching ratio of each scattering point in Fig. 5 is equal to 1, so the novel WDA has achieved accurate focusing for all scattering points in Fig. 5. Observing Fig. 4 and Fig. 5, it is clear that the novel WDA has almost the same imaging effect with BPA. However, their computation complexities are different. Let $I(\mathbf{P})$ denote SAR image of the scattering point $\mathbf{P}$. Assume that the size of $I(\mathbf{P})$ and the size of received data are both $N \times N$. The complexity of BPA is about $O(N^3)$, but that of the novel WDA is only $O(N^2 \log_2 N)$. This practical experiment shows that the novel WDA can well deal with the measured data in practice, and it also verifies the effectiveness and correctness of our novel algorithm.

Table 2. System parameters for airborne BiSAR.

System parameters	Transmitter	Receiver
Initial position (m)	$(125, -965, 300)$	$(-125, -715, 300)$
Platform velocity (m/s)	$(151.3958/3.6, 0, 0)$	
Carrier frequency (GHz)	9.618	
Sampling frequency (MHz)	120	
Range bandwidth (MHz)	80	
Pulse width (us)	20	
Pulse repetition frequency (Hz)	500	

5. CONCLUSION

In this paper, we first propose an equivalent monostatic model for BiSAR. Based on this model, a novel imaging algorithm for BiSAR in wavenumber domain is further established. Because of solving system of linear equations can be easily carried out in mathematics, the proposed algorithm has strong operability in practice. It makes us handle the echo data of BiSAR in the manner of traditional monostatic SAR. The imaging results of simulation and practical experiment have validated that the proposed algorithm can well focus the echo data of BiSAR, and meanwhile its computation complexity is lower than back projection algorithm. In addition, the equivalent monostatic model can be also extended to other BiSAR imaging algorithms.

ACKNOWLEDGMENT

REFERENCES

1. Huang, J. Q., Q. Wang, and W. Q. Wu, "Motion compensation in SAS with multiple receivers based on range-Doppler imaging algorithm," *International Conference on Electric Information and Control Engineering*, 1476–1479, 2011.

2. Guan, J., H. X. Wang, M. Fan, and J. Wang, "The application of range Doppler algorithm for side-looking strip-map SAS," *IEEE International Conference on Signal Processing, Communication and Computing*, 1–4, 2013.

3. Di Lorenzo, P., S. Barbarossa, and L. Borgarelli, "Optimal beamforming for range-Doppler ambiguity minimization in squinted SAR," *IEEE Transactions on Aerospace and Electronic Systems*, Vol. 49, No. 1, 277–293, 2013.

4. Li, D., G. S. Liao, W. Wang, and Q. Xu, "Extended azimuth nonlinear chirp scaling algorithm for bistatic SAR processing in high-resolution highly squinted mode," *IEEE Geoscience and Remote Sensing Letters*, Vol. 11, No. 6, 1134-1138, 2014.

5. Chen, S. C., M. D. Xing, T. L. Yang, and Z. Bao, "A nonlinear chirp scaling algorithm for tandem bistatic SAR," *IEEE International Geoscience and Remote Sensing Symposium*, 2485–2488, 2013.

6. Xu, W., P. P. Huang, R. Wang, Y. K. Deng, and Y. C. Lu, "TOPS-mode raw data processing using chirp scaling algorithm," *IEEE Journal of Selected Topics in Applied Earth Observations and Remote Sensing*, Vol. 7, No. 1, 235–246, 2014.

7. Wang, R., O. Loffeld, H. Nies, S. Knedlik, M. Hagelen, and H. Essen, "Focus FMCW SAR data using the wavenumber domain algorithm," *IEEE Transactions on Geoscience and Remote Sensing*, Vol. 48, No. 4, 2109–2118, 2010.

8. Liang, X. T. and Q. Wei, "Wavenumber domain algorithm for squint FMCW SAR," *International Forum on Strategic Technology*, Vol. 2, 1256–1260, 2011.

9. Li, Z. Y., J. J. Wu, Q. Y. Yi, Y. L. Huang, and J. Y. Yang, "A wavenumber-domain imaging algorithm for spaceborne/airborne hybrid bistatic SAR," *IEEE Radar Conference*, 1–5, 2013.

10. Rhode, S., K. Usevich, I. Markovsky, and F. Gauterin, "A recursive restricted total least-squares algorithm," *IEEE Transactions on Signal Processing*, Vol. 62, No. 21, 5652–5662, 2014.

11. Rhode, S. and F. Gauterin, "Online estimation of vehicle driving resistance parameters with recursive least squares and recursive total least squares," *IEEE Intelligent Vehicles Symposium*, 269–276, 2013.

12. Cumming, I. G. and F. H. Wong, *Digital Signal Processing of Synthetic Aperture Radar Data: Algorithms and Implementation*, Artech House, Boston, USA, 2004.

13. Zhang, P., X. Zhang, and G. Fang, "Comparison of the imaging resolutions of time reversal and back-projection algorithms in EM inverse scattering," *IEEE Geoscience and Remote Sensing Letters*, Vol. 10, No. 6, 357–361, 2013.

14. Zhang, L., H. Li, and Z. Xu, "A fast BP algorithm with wavenumber spectrum fusion for high-resolution spotlight SAR imaging," *IEEE Geoscience and Remote Sensing Letters*, Vol. 11, No. 9, 1460–1464, 2014.

15. Wang, Y., X. Zhang, W. Li, and J. Shi, "A new bistatic-based sparse linear array 3D imaging SAR model," *IEEE International Geoscience and Remote Sensing Symposium*, 463–466, 2008.